International Journal of Biological Macromolecules 103 (2017) 467–476

Contents lists available at ScienceDirect

International Journal of Biological Macromolecules

journal homepage: www.elsevier.com/locate/ijbiomac

Nanocellulose-collagen-apatite composite associated with osteogenic growth peptide for bone regeneration

Sybele Saska[a,*], Lucas Novaes Teixeira[b], Larissa Moreira Spinola de Castro Raucci[b], Raquel Mantuaneli Scarel-Caminaga[c], Leonardo Pereira Franchi[d], Raquel Alves dos Santos[d], Silvia Helena Santagneli[a], Marisa Veiga Capela[a], Paulo Tambasco de Oliveira[b], Catarina Satie Takahashi[d], Ana Maria Minarelli Gaspar[c], Younès Messaddeq[a], Sidney José Lima Ribeiro[a], Reinaldo Marchetto[a]

[a] São Paulo State University, UNESP, Institute of Chemistry, Araraquara, São Paulo, Brazil
[b] Cell Culture Laboratory, Faculty of Dentistry of Ribeirão Preto, University of São Paulo, USP, Ribeirão Preto, São Paulo, Brazil
[c] São Paulo State University, UNESP, School of Dentistry at Araraquara, São Paulo, Brazil
[d] Department of Genetics, Faculty of Medicine of Ribeirão Preto, University of São Paulo, USP, Ribeirão Preto, São Paulo, Brazil

ARTICLE INFO

Article history:
Received 13 February 2017
Received in revised form 12 April 2017
Accepted 16 May 2017
Available online 18 May 2017

Keywords:
Bacterial cellulose
Composite
Tissue engineering
Bone regeneration
Peptide
Biopolymer

ABSTRACT

Despite advances in the field of biomaterials for bone repair/regeneration, some challenges for developing an ideal bone substitute need to be overcome. Herein, this study synthesized and evaluated *in vitro* a nanocomposite based on bacterial cellulose (BC), collagen (COL), apatite (Ap) and osteogenic growth peptide (OGP) or its C-terminal pentapeptide [OGP(10-14)] for bone regeneration purposes. The BC-COL nanocomposites were successfully obtained by carbodiimide-mediated coupling as demonstrated by spectroscopy analysis. SEM, FTIR and ^{31}P NMR analyses revealed that *in situ* synthesis to apatite was an effective route for obtaining of bone-like apatite. The OGP-containing (BC-COL)-Ap stimulated the early development of the osteoblastic phenotype. Additionally, the association among collagen, apatite, and OGP peptides enhanced cell growth compared with OGP-containing BC-Ap. Furthermore, none of the nanocomposites showed cytotoxic, genotoxic or mutagenic effects. These promising results suggest that the (BC-COL)-Ap associated with OGP peptides might be considered a potential candidate for bone tissue engineering applications.

1. Introduction

Alloplastic materials have achieved great progress for bone substitutes in the development of bioceramics, bioactive glasses and polymers [1]. Despite advances in biomaterials synthesis for bone tissue engineering applications is still investigated a material, which can comprise osteoconductive and osteoinductive properties. Moreover, these materials should preferably have a surface structure closer to the natural extracellular matrix (ECM) for improving cell/material interactions, besides good mechanical property in order to promote an effective and predictable bone repair/regeneration.

Furthermore, the increasing demand for materials from renewable and nontoxic sources has motivated extensive studies from bacterial cellulose (BC) as a promising biopolymer for biomedical applications as tissue engineering scaffolds [2,3]. Additionally, the nanofibrillar structure of BC is similar to ECM, which makes this biopolymer to be further promising for tissue engineering and regenerative medicine applications.

BC or nanocellulose plays a fundamental role in this scenario becoming an important biotechnological product for health and for industry. Nanocellulose obtained from cultures as *Gluconacetobacter xylinus, Gluconacetobacter hansenii or Gluconacetobacter kombuchae* is free of lignin and hemicelluloses as well as other biogenic products. Additionally, BC presents higher molecular weight and crystallinity than plant cellulose [2]. Nanocellulose synthesized in static culture results in a three-dimensional structure consisting of an ultrafine network of cellulose nanofibers differently than plant

* Corresponding author at: São Paulo State University, UNESP, Institute of Chemistry, PC 355 Araraquara, São Paulo, Brazil.
E-mail addresses: sysaska@gmail.com (S. Saska), novaesrp@yahoo.com.br (L.N. Teixeira), larissa_spinola@yahoo.com.br (L.M.S. de Castro Raucci), raquel@foar.unesp.br (R.M. Scarel-Caminaga), leonardofranchi@yahoo.com.br (L.P. Franchi), rasantosgen@yahoo.com.br (R.A. dos Santos), santagneli@iq.unesp.br (S.H. Santagneli), marisavc@iq.unesp.br (M.V. Capela), tambasco@usp.br (P.T. de Oliveira), cstakaha@usp.br (C.S. Takahashi), anamaria@foar.unesp.br (A.M.M. Gaspar), younes.messaddeq@copl.ulaval.ca (Y. Messaddeq), sidney@iq.unesp.br (S.J.L. Ribeiro), marcheto@iq.unesp.br (R. Marchetto).

http://dx.doi.org/10.1016/j.ijbiomac.2017.05.086
0141-8130/

cellulose, in which cellulose fibers are micrometer size. Moreover, BC compared with plant cellulose and other natural resorbable polymers presents high mechanical properties, which are essential for barrier membranes and scaffolds in tissue repair [4,5]. BC has been used as an excellent matrix for synthesis of biomaterials for tissue engineering and regenerative medicine applications associated with hydroxyapatite (HA) or other apatite phases (Ap) [6–11], or associated with organic components of bone extracellular matrix or other biopolymers and biomolecules such as: collagen [5,12–14], gelatin [11,15], silk fibroin [16] and peptides or growth factors [17–21].

Bioactive-polymeric materials have demonstrated to be potential candidates to improve the biological and mechanical properties in bone tissue engineering, mainly composites based on HA and collagen have shown good results of biological/mechanical properties and chemical stability [22,23]. Indeed, alloplastic materials containing HA and collagen are bone substitutes of choice due to their physicochemical features similar to bone tissue besides them can be effective and predictable materials in bone repair/regeneration [24,25]. Collagen is the most abundant protein in the ECM and in the human body, which is a bioactive molecule may improve the biological properties of materials stimulating a better regeneration process. *In vivo* and *in vitro* studies have shown the key role of collagen molecules to different composites [26,27]. In addition, synthetic biomolecules has been widely used to improve the bioactivity of biomaterials, owing of being easily identified and bound to specific sites on ECM and hence increasing the cell-material interaction [28]. In this context, osteogenic growth peptide (OGP) and its C-terminal pentapeptide [OGP(10-14)] were chosen as biomolecules for improving osteoconductive and osteoinductive properties of the synthesized composites. OGP is identical to the C-terminal amino acid sequence of histone H4. This sequence is physiologically present in mammalian serum mainly as an OGP-OGP binding proteins (OGPBP) complex [29,30]. The concentration of serum OGP is increased transiently during a local injury to bone tissue, bone marrow or systemic osteogenic reactions or in the event of low doses of exogenous OGP. Thereby, OGP is required for stimulation of bone formation, suggesting a self-regulatory function for complexes OGPBPs [29,31,32]. The regulatory role of OGP and its derivatives, such as the OGP(10-14), is to promote osteogenesis and hematopoiesis in proliferation and differentiation of osteoprogenitor cells and hematopoietic progenitor cells. Additionally, these peptides promote bone formation and the increase of trabecular bone density, and stimulate fracture healing when systemically administered [33–35]. OGP-containing biomaterials have exhibited an increase of the osteoblast differentiation/activity as a result a better bioactivity of these biomaterials and a positive effect on bone healing [21,36–38].

Hence, this study aimed to synthesize an organic-inorganic composite based on collagen covalently bonded to the BC network and then apatite phase and OGP or OGP(10-14) peptides were incorporated to the BC-COL composites conferring upon them bioactive and osteoinductive properties. Considering our previous studies, the BC-COL composite demonstrated higher levels of ALP activity although has shown a delay in the matrix mineralization [14]; moreover, OGP-free BC-HA composite or OGP-containing BC-HA composite showed to be biocompatible and effective for bone regeneration in bone defects of rat tibiae [10] or in critical-size mice calvarial defects [21], respectively. Furthermore, OGP peptides influenced the osteogenic proliferation and favored the mineralization process, conferring an osteoinductive property to the BC membrane [18]. Taken together, inorganic phase and OGP peptides when associated with the BC-COL composite is expected these compounds may promote an earlier osteogenic differentiation. Therefore, osteoinductive potential in early osteogenesis as well as cytotoxic, genotoxic and mutagenic effects were evaluated on the (BC-COL)-Ap composites associated with OGP and OGP(10-14) peptides.

2. Experimental

2.1. Synthesis of the (BC-COL)-Ap nanocomposite

BC membranes were obtained from cultures of wild strains of *Gluconacetobacter xylinus*, which were cultivated in culture medium contianing 2 wt% glucose, 0.5 wt% peptone, 0.5 wt% yeast extract, 0.27 wt% disodium hydrogen phosphate, and 0.115 wt% citric acid for 120 h at 28 °C in static culture. BC pellicles were formed at the air/liquid interface and then were harvested, and purified by immersion in a 2 wt% NaOH solution at 80 °C for 1 h; subsequently the pellicles were immersed in a 1 wt% NaClO solution for 30 min. These pellicles were then washed with deionized water and sterilized (120 °C for 15 min). Highly hydrated BC membranes were cut into a standard size: 25 mm in diameter and 5-mm thick. BC samples were prepared for mechanical testing wherein these samples were dried at 50 °C and sterilized by gamma radiation (25 kGy).

The synthesis of the BC-COL composites was performed using carbodiimide coupling to bind collagen to the glycine-modified BC following the methodology previously proposed by Saska et al. [14]. First, the BC was modified by glycine (Gly) esterification to the free hydroxyl groups, through a solid-phase synthesis strategy employing Fmoc-based chemistry (9-fluorenylmethyloxycarbonyl, Fmoc). The esterification reaction was performed using a solution containing 0.7 mol L^{-1} Fmoc-Gly, 0.1 mol L^{-1} 1,1′-cabonyldiimidazole (CDI) (Sigma®), 0.02 mol L^{-1} N-methylimidazole (NMI) (Fluka®) in dimethylformamide (DMF) (Synth®) under shaking at room temperature (RT) for 2 h. Quantitative analysis by ultraviolet-visible spectroscopy (UV/VIS, SHIMADZU UV-1601PC; detection at 290 nm) was used to determine the incorporation degree of Fmoc-Gly to the OH groups of BC after deprotection of Fmoc groups using a soultion of 20% piperidine in DMF (v/v).

Gly-modified BC samples were soaked into 4 mmol L^{-1} collagen aqueous solution (type I collagen from rat tail tendon, Sigma®) to carbodiimide-mediated coupling wherein 5 mmol L^{-1} 1-ethyl-3-(3-dimethylaminopropyl) carbodiimide (Novabiochem®) were added to collagen solution at 4 °C. The samples were rinsed with deionized water under vacuum to remove excess reagents.

Apatite incorporation into the BC-COL composites was performed by *in situ* precipitation. The BC-COL samples were separately immersed into 0.05 mol L^{-1} $CaCl_2$ solution and then into 0.1 mol L^{-1} Na_2HPO_4 solution at RT for 24 h each immersion [10]. The (BC-COL)-Ap samples were dried at 37 °C for obtaining of the membrane-shaped (BC-COL)-Ap nanocomposites and then sterilized by gamma radiation (25 kGy).

2.2. Incorporation of peptides into samples

OGP (H_2N-ALKRQGRTLYGFGG-OH) and OGP(10-14) (H_2N-YGFGG-OH) peptides were synthesized manually by the solid-phase method (synthesis and characterization of both peptides are described in Supplemental Material).

Incorporation of the peptides was performed by adsorption into the (BC-COL)-Ap nanocomposites and control samples (BC-Ap nanocomposite) for *in vitro* assays. BC-Ap nanocomposites were prepared in accordance with previous methodology described by Saska et al. [10]. The peptide concentration to be incorporated the samples was determined from the values obtained in the OGP peptide release (data not shown). Thereby, the (BC-COL)-Ap and BC-Ap nanocomposites of 13 mm in diameter and 5-mm thick were immersed in 5 mL 10^{-8} mol L^{-1} peptide solution, OGP or OGP(10-

14), for 72 h at 10 °C. Afterwards, each sample was dried at 37 °C and then sterilized by gamma radiation (25 kGy).

2.3. (BC-COL)-Ap nanocomposite characterizations

Scanning electron microscopy (SEM) images were obtained with a Philips XL 30 scanning electron microscope. The samples were sputter-coated with a 1-nm thick gold layer for 60 s (3 kV and 9.5 μA). The morphology of the samples was observed at an accelerating voltage of 5 kV. Fourier transform infrared (FTIR) spectra were obtained from dried powdered samples on a Perkin Elmer Spectrum 2000 Fourier transform infrared spectrophotometer. Pellets were prepared from mixtures of the samples and KBr (1:100 in weight). Thirty-two scans were accumulated at a resolution of 4 cm^{-1}. ^{31}P Nuclear Magnetic Resonance (^{31}P NMR) solid state experiments were measured at 121.5 MHz on a Varian Unit INOVA 300 spectrometer using a 7 mm CP-MAS-NMR probe at a spinning speed of 6 kHz at room temperature. 90° pulses of 7 μs length and recycle delays of 200 s were used. The spinning frequency [magic-angle sample spinning (MAS)] was 6 kHz. Chemical shifts are reported relative to 85% H_3PO_4. Signal deconvolutions into Gaussian components were done using the DMFIT software package [39]. Thermogravimetric (TG) curves of the dried samples were recorded using a TA SDT 2960 from TA Instruments Co. Samples were heated in open α-alumina pans from 25° to 600 °C under a nitrogen atmosphere (flow rate: 70 mL min^{-1}) at a heating rate of 10 °C min^{-1}. Mechanical properties, including tensile strength, elastic modulus and strain at failure of BC, BCγ, (BC-COL)-Ap and (BC-COL)-Apγ membranes were carried out on a MTS-810 testing machine (Material Test System – MTS 810; MTS System Corporation) equipped with Test Star II software, a 10-kN load cell and a tensile force applied at an extension rate of 0.5 mm min^{-1}. The BC and (BC-COL)-Ap membranes with thicknesses in the range of 40-μm and 160-μm, respectively were cut into regular rectangular shapes with an inner width of 7.50 mm. At least five specimens were tested for each condition. Before the measurement, each sample was immersed in simulated body fluid for 10 min at RT. After 10 min, the samples were laid on filter paper for remove excess superficial water before carrying out the mechanical testing. Tensile strength was determined as the maximum point of the force-strain curve.

The (BC-COL)-Ap and (BC-COL)-Ap OGP(10-14) samples were used before or after sterilization by gamma radiation (γ), whereas the type of peptide molecule does not interfere in the characterization techniques performed in this work.

2.4. Cell culture experiments

In vitro assays methodologies are described in Supplementary Material.

2.5. Statistical analysis

Shapiro-Wilk test was used to assess the normality of the data and Levene's test for homogeneity. In view of the results, parametric tests were utilized. Analysis of variance (ANOVA) followed by Tukey's test. Statistica 8.0 software was used to perform the tests. Differences were considered statistically significant when $p < 0.05$. Data from treated groups of cytotoxicity, genotoxicity and mutagenicity assays were compared with the negative control of their experiments. The experimental results are expressed as mean and standard error. All assays were performed in duplicate.

3. Results and discussion

3.1. Physicochemical and mechanical properties of the (BC-COL)-Ap nanocomposites

Fig. 1 shows SEM images of the BC membrane and of the (BC-COL)-Ap and (BC-COL)-Ap OGP(10-14) nanocomposites. Fig. 1A

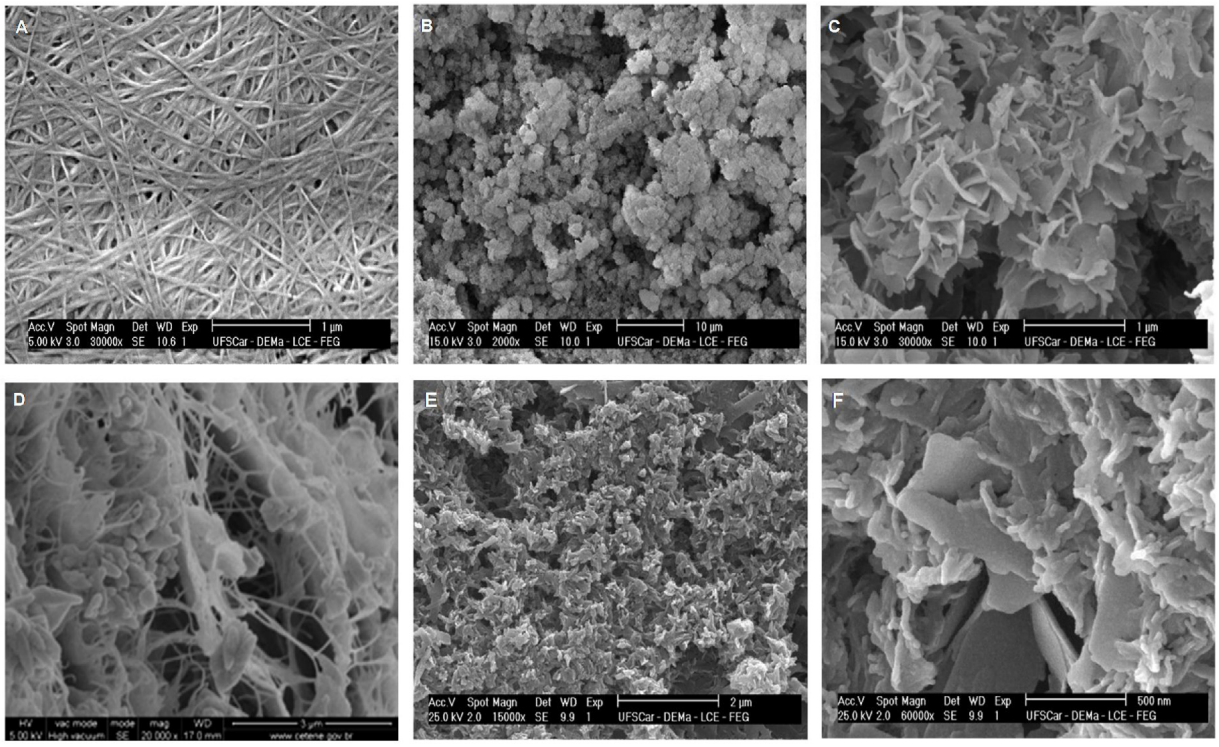

Fig. 1. SEM surface images of the BC membrane (A) and of the (BC-COL)-Ap nanocomposite (B, C); SEM cross-section images of the (BC-COL)-Ap nanocomposite (D); SEM surface images of the (BC-COL)-Ap OGP(10-14) nanocomposite (E, F).

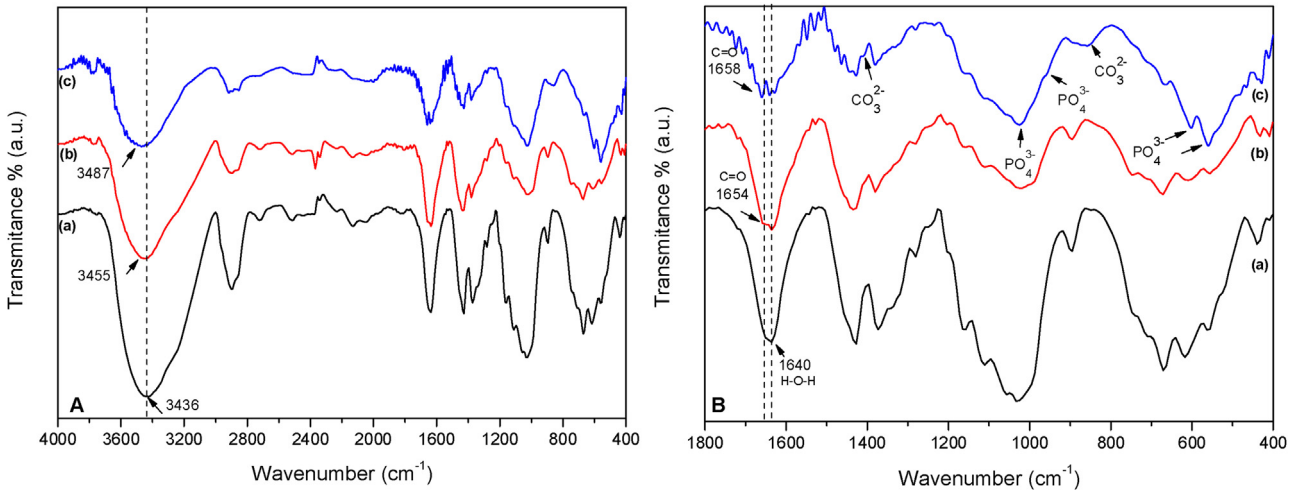

Fig. 2. FTIR spectra (A): BC membrane (a), BC-COL composite (b) and (BC-COL)-Ap composite (c). FTIR spectra (B): spectra around 1800–400 cm^{-1} show the band at 1640 cm^{-1} of the BC spectrum (a) attributed to the amide I band (C=O stretching of proteins – dashed line) comparing to the red shift at 1654 cm^{-1} (b) and at 1658 cm^{-1} (c); characteristic Ap bands correspond to PO_4^{3-} and CO_3^{2-} ions (arrows) at spectrum (c).

shows a well-organized three-dimensional (3D) structure of the BC membrane. SEM image of the (BC-COL)-Ap nanocomposite shows the surface homogeneously covered by Ap nanocrystals (Fig. 1B, C). Ap nanocrystals were uniformly precipitated on the BC-COL composite as spherical agglomerates (Fig. 1B). Higher magnifications revealed that the spherical particles were composed of discrete crystallites with a needle-like or plate-like morphology (Fig. 1C), characteristic of the octacalcium phosphate phase (OCP) [6,40] even though these crystallites showed a more rounded shape than a pure crystal of OCP. These morphological aspects showed the apatite crystals providing secondary nucleation sites for additional apatite formation [6]. The reduction of crystal size might be owing to the substitution of PO_4^{3-} ions by CO_3^{2-} ions, resulting in the change of crystal morphology. Indeed, the type B substitution of CO_3^{2-} (carbonate apatite) results in a decrease in the crystal size, by more than one order of magnitude, and in a morphological change from needle-like to rods and then to equiaxial crystals (spheroids) [41]. This morphology corroborated to HA-crystals morphology observed inside composite, which presented in globular shape, similar to the crystals of calcium-deficient hydroxyapatite (CDHA) or carbonate apatite (Fig. 1D).

Furthermore, the presence of peptides may stimulate nucleation and growth of nanocrystalline inorganic phase similar to bone apatite and carbonate apatite in the shape of elongated plate-like [42]. Therefore, the presence of collagen and peptides induced the formation of HA crystals with morphology similar to carbonate apatite. SEM image obtained from (BC-COL)-Ap OGP(10-14) nanocomposite (Fig. 1E, F) shows the peptide incorporation changed the surface morphology promoting the formation of agglomerates of small apatite crystals, such as plate-like and rod-like crystallites (Fig. 1F). Moreover, the observed morphology to apatite was quite similar to the apatite crystals found in human woven bone [43]. Thereby, the (BC-COL)-Ap nanocomposite immersed into peptide solution induced the formation of plate-like and rod-like crystallites whereas these morphologies are corresponding to CDHA or carbonate apatite phases.

Typical IR bands to cellulose were observed (Fig. 2A): OH stretching at 3450 cm^{-1}, CH stretching for the alkanes and CH_2 asymmetric stretching at ~2900 cm^{-1}, CH_2 symmetric stretching at 2700 cm^{-1}, H—O—H bending of adsorbed water at 1640 cm^{-1}, CH_2 deformation at 1432 cm^{-1}, CH_3 deformation at ~1370 cm^{-1}, OH deformation at ~1332 cm^{-1} [10]. At the region around 3450 cm^{-1} was observed an intense band in all IR spectra, but this band was less intense in the BC-COL and (BC-COL)-Ap samples, respectively. The decrease in the intensity of this band and the red shift (19 cm^{-1}) observed to the BC-COL suggests the amino acid Gly was bonded to the OH groups of BC by hydrogen bonding. Moreover, this result suggets that the collagen was bonded to the free OH groups of the Gly-modified BC by carbodiimide-mediated coupling. A red shift of 55 cm^{-1} in comparison with BC and of 32 cm^{-1} in comparison with the BC-COL composite was also observed. The decrease in the intensity and the red shift suggested presence of the apatite crystals interacted with OH groups from the BC or collagen. In addition, the red shift observed at the band attributed to intramolecular hydrogen bonding (~3500 cm^{-1}) confirmed strong interaction between the OH group and apatite.

The spectral region attributed to the amide I protein band was observed as an overlapped with the adsorbed water band (H—O—H bending) at 1640 cm^{-1}. The bonded collagen to BC was attributed to the shifting of the band at 1640 cm^{-1}–1654 cm^{-1} (Fig. 2B). Additionally, in the BC-COL and (BC-COL)-Ap spectra a weak band was observed at 1658 cm^{-1}.

Typical IR bands to PO_4^{3-} ions stretching associated with apatite phases were observed at 1093, 1024, 560–600 cm^{-1} [6,44]. The 962 cm^{-1} band showed as a shoulder of the stronger band at the 1024 cm^{-1}. The weak bands at 1412 and 855 cm^{-1} were attributed to stretching of CO_3^{2-} ions (Fig. 2B). The presence of the strong bands of PO_4^{3-} at 605 and 567 cm^{-1} suggested the precursor phase of HA was the OCP phase [45]. The (BC-COL)-Ap spectrum showed broader bands suggesting the presence of HA crystals of low crystallinity, in agreement with SEM and ^{31}P NMR data. Therefore, FTIR analysis suggested the formation of bone-like apatite on BC nanofibers.

^{31}P NMR results obtained from BC-Ap and (BC-COL)-Ap composites elucidated the apatite phases precipitated into the composites. Fig. 3A shows ^{31}P NMR spectra measured from the BC-Ap and (BC-COL)-Ap samples. Fig. 3B shows the corresponding deconvolutions procedure. The deconvolution from spectrum BC-Ap spectrum suggested the contribution of three different phophate groups (Fig. 3B). The peak at 3.2 ppm can be attributed the crystalline phase of CDHA [46,47]; moreover, the CDHA phase can be related to an apatite phase present in transition of OCP to HA phase [46]. Whereas HA and OCP have similarity structural suggesting the hypothesis of OCP to be a precusor phase as biological apatite [48] as synthetic HA [49]. Legeros [50] related the change of phases, amorphous calcium phosphate (ACP), dicalcium phosphate dihydrate (DCPD –

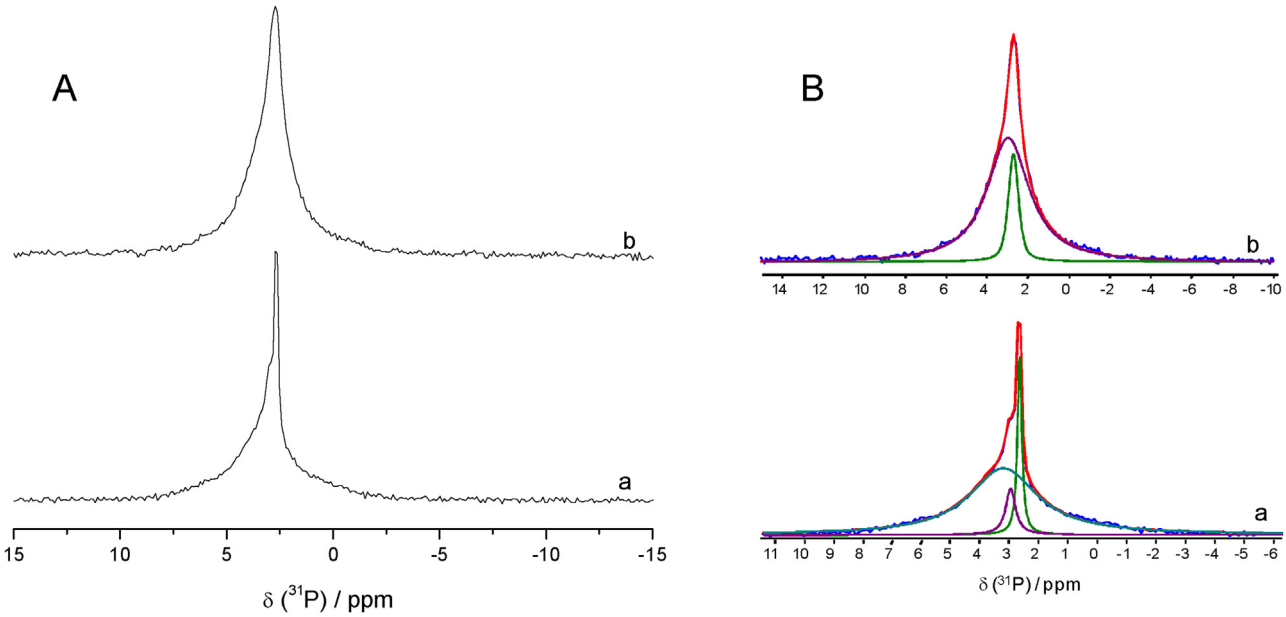

Fig. 3. A: Solid-sate ^{31}P MAS NMR spectra of the BC-Ap (a) and (BC-COL)-Ap (b) composite; B: corresponding deconvolutions to spectra, BC-Ap (a): green line: 2.7 ppm; purple line: 2.9 ppm; blue line: 3.2 ppm; (BC-COL)-Ap (b): green line: 2.7 ppm; purple line: 2.9 ppm. (For interpretation of the references to colour in this figure legend, the reader is referred to the web version of this article.)

brushite), dicalcium phosphate (DCP – monetite) or OCP to HA in solutions contanining Ca^{2+} ions or only Pi, resulting in the formation of CDHA with HPO_4^{2-} ions incorporation. Hence, in the present study, Na_2HPO_4 solution used to apatite precipitation was able to supply HPO_4^{2-} ions during this process and to afford the formation of CDHA phase. Indeed, the results demonstrated that CDHA phase was predominant (77%) in the BC-Ap composite. Furthermore, the peak at 2.9 ppm can be attributed to the presence of carbonate ions characterizing a phase of impure apatite, type-B carbonate apatite [42,47,51] wherein might result in a ^{31}P chemical shift compared with HA. Thereby, the peak observed at 2.9 ppm was attributed to carbonate apatite and the peak at 2.7 ppm was attributed to HA crystalline phase [51].

Fig. 3B shows a broad and asymmetric peak at 2.8 ppm to (BC-COL)-Ap. Deconvolution process has lead to the contribution of two different phophate groups. The broad peak at 2.9 ppm can be attributed to carbonate apatite [42,47,51]. The sharp peak at 2.7 ppm can be attributed to HA crystalline phase [51]. Overall, these results demonstrated that two-apatite phase precipitation in the (BC-COL)-Ap nanocomposite, carbonate apatite (84%) and HA crystalline (16%) distributed on BC fibers and collagen.

The CO_3^{2-} substitution at the PO_4^{3-} site in HA crystals is commonly observed for preparations in aqueous systems [42]. The substitution of PO_4^{3-} ions by CO_3^{2-} ions in the type-B carbonate apatite can influence simultaneously the presence of other cations, as substitution of Ca^{2+} ions by Na^+ ions. These substitutions might occur by direct precipitation or by hydrolysis of ACP, brushite, monetite or OCP in a solution containing carbonate. This feature also promote decrease in crystal size, change in crystal morphology, higher solubility and decrease in the Ca/P molar ratio [50]. In addition, the presence of collagen in the composites might afford the carbonate-apatite formation, whereas the amino acids have shown to promote the change of OCP to HA [52] or to afford the inorganic-phase precipitation, due to interactions between amino acids with the cationic or anionic components present on the mineral surface [53]. The data ^{31}P NMR to this composite corroborated to the results observed in the SEM and FTIR data.

Thermogravimetric analysis was performed to estimate the thermal stability and degradation profiles the BC, (BC-COL)-Ap and (BC-COL)-Ap OGP(10-14) samples before and after sterilization by gamma radiation (γ). In general, all samples showed an initial smooth loss in weight from a 25 up to 250 °C (8 up to 10%) due to water and solvent loss [44]. An important weight loss was observed at around 267 °C up to 308 °C (decomposition temperature: T_{onset}), as shown in Table 1. This event could be associated with cellulose degradation including depolymerization, dehydration and decomposition of glucosyl units followed by the formation of a charred residue [44], which correspond to around 23% of the carbonaceous residue at 600 °C of the BC samples (Fig. 1S). Moreover, T_{onset} observed in the TG curves revealed that the thermal stability of BC slightly increased following the gamma radiation (T_{onset}: BC = 289 °C; BCγ = 308 °C). Compared with the BC membrane T_{onset}, the collagen and apatite incorporation promoted a slight increase in the thermal stability of the composites before sterilization (T_{onset}: (BC-COL)-Ap = 302 °C; (BC-COL)-Ap OGP(10-14) = 303 °C). This increase in the thermal stability might be related to formation of hydrogen bonding due to apatite precipitation [54] or by structural changes related to collagen incorporation into the BC as observed in the XRD results (Fig. 2S). These compounds might also hinder the gas permeation by formation of a barrier. In addition, the T_{onset} values to the (BC-COL)-Ap and (BC-COL)-Ap OGP(10-14) composites were similar even after sterilization (Table 1). Furthermore, the thermal stability of the composites did not change by gamma radiation. Thus, indicating that gamma radiation is an adequate treatment for sterilization.

Mechanical properties, such as tensile strength (σ), elastic modulus (*E*), and strain at failure (ε), are summarized in Table 2. The

Table 1
Decomposition temperatures (T_{onset}) of the BC membrane and of the (BC-COL)-Ap and (BC-COL)-Ap OGP(10-14) nanocomposites before or after the process of sterilization by gamma radiation.

	T_{onset} (°C)	
Samples	before sterilization	after sterilization
BC	289	308
(BC-COL)-Ap	302	300
(BC-COL)-Ap OGP(10-14)	303	300

Table 2
Mechanical properties of the BC and (BC-COL)-Ap membranes (before and after sterilization by gamma radiation). The values represent mean ± error standard, where n = 5.

Sample	σ (MPa)	ε (%)	*E* (GPa)
BC	95.1 ± 4.6	11.8 ± 0.5	0.9 ± 0.03
BCγ	83.5 ± 6.0	7.8 ± 0.8	1.13 ± 0.1
(BC-COL)-Ap	57.7 ± 1.8	21.6 ± 2.6	0.27 ± 0.03
(BC-COL)-Apγ	45.0 ± 4.0	10.8 ± 1.7	0.45 ± 0.07

results revealed that the collagen and apatite incorporation into the BC network increased the strain at failure, despite the decrease in tensile strength and elastic modulus when compared with the BC membranes. Although gamma radiation decreased the strain at failure in both samples, the (BC-COL)-Apγ showed a higher value to strain at failure than the BCγ. However, the decrease in the elongation observed in the samples might be related to the BC network, and not in relation to the collagen or apatite incorporation to the BC. In the BCγ can be observed a decrease of 66% compared with BC, and this pattern was also maintained to the (BC-COL)-Apγ showing a decrease in 50% (Table 2).

These results suggest that the collagen and inorganic phase in the BC network promoted a better flexibility than in BC membranes even after sterilization. This factor can favor the handling of these membranes in surgical applications. The mechanical properties of the (BC-COL)-Ap nanocomposites were greatly higher than other composites based on collagen and HA [24,27]. Moreover, commercial collagen membranes have also shown low values for tensile strength and elastic modulus when compared with the mechanical properties of the (BC-COL)-Ap nanocomposite [55]. Therefore, BC was an excellent template for the incorporation of collagen and apatite, considering that lower collagen amount of this composite than commercial membranes and other composites [24,27,55]. In addition, these results revealed that the (BC-COL)-Ap nanocomposite represented a great advance in relation to mechanical properties, when collagen and apatite are used to the preparation of the membranes.

3.2. In vitro *assays*

The cytotoxicity, genotoxicity and mutagenic results are shown in Supplementary Material.

3.2.1. *Evaluation of cell morphology, of cell viability/proliferation, total protein content and ALP activity*

Clinical success for application of drug delivery systems is related to some features such as optimal-therapeutic dose and a good specific carrier to a determined drug. Indeed, these features were observed in this *in vitro* study, wherein the (BC-COL)-Ap nanocomposites demonstrated to be good carriers for OGP peptides. Additionally, the optimal concentration for both peptides, OGP and OGP(10-14) is 10^{-9} mol L^{-1} to *in vitro* studies [29,56].

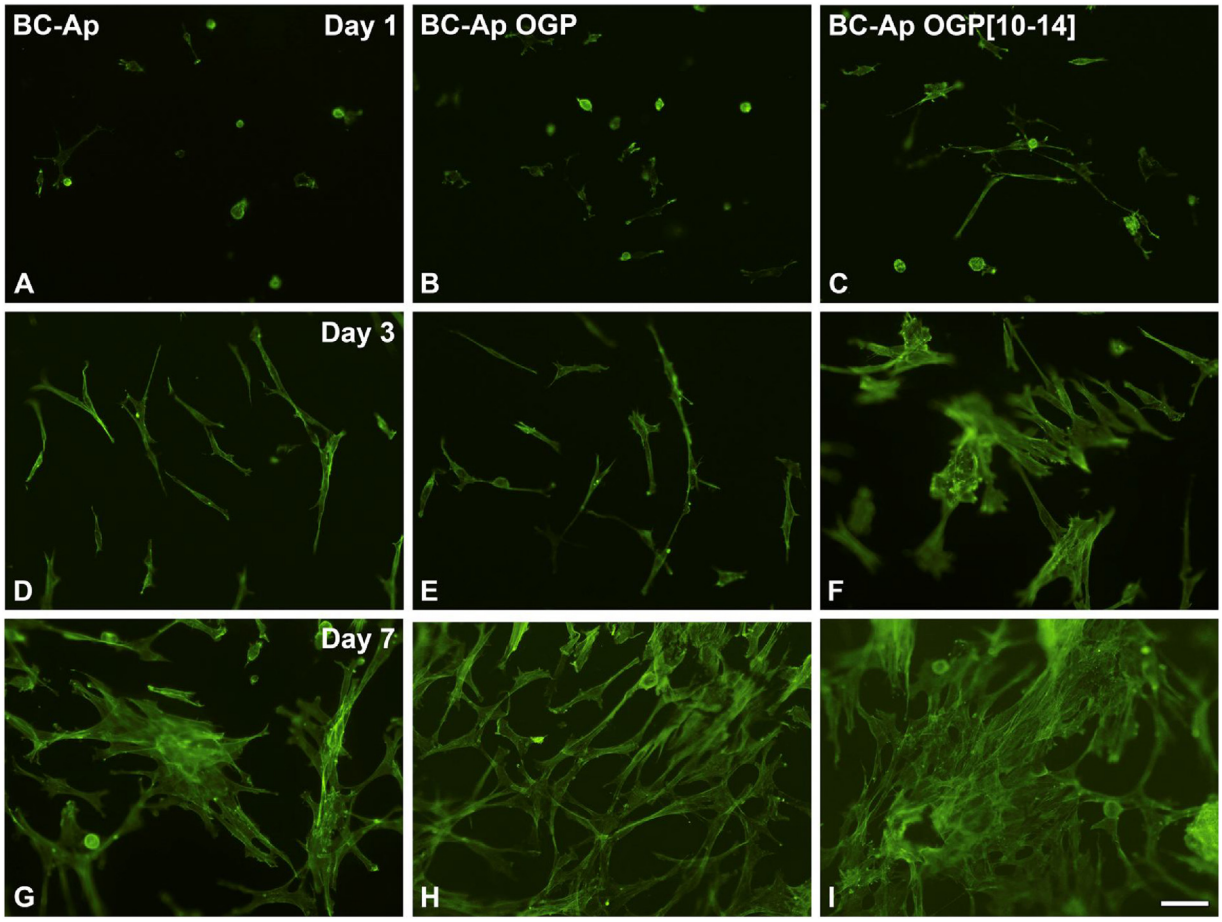

Fig. 4. Epifluorescence of osteoblastic cells cultured on BC-Ap (A, D, G) BC-Ap OGP (B, E, H), and BC-Ap OGP(10-14) (C, F, I) at 1 (A-C), 3 (D–F), and 7 (G-I) days. Green fluorescence (Alexa Fluor 488-conjugated phalloidin) reveals actin cytoskeleton. At day 1, the cells cultured on BC-Ap, BC-Ap OGP were adhered and exhibited predominantly cell roundish morphology, while those ones grown on BC-Ap OGP(10-14) showed a spread morphology (Compare C to A and B). At day 3, cell spreading was observed for all membranes (D-F). At day 7, a moderately greater cell population was noticed on BC-Ap OGP and BC-Ap OGP(10-14) (compare B and C to A). Bar: A–F = 100 μm. (For interpretation of the references to colour in this figure legend, the reader is referred to the web version of this article.)

Herein, the incorporated therapeutic dose to the samples of 10^{-8} mol L^{-1} was efficient for inducing *in vitro* early development of osteoblastic phenotype, considering that the released peptide concentration was around 10^{-9} mol L^{-1} (data not shown).

BC membrane has several features that make it a suitable alternative for guided bone regeneration (GBR) procedures [4,5]. Nevertheless, BC association with other bioactive materials may improve its mechanical and biological properties [8,10,14]. Thereby, morphological analysis showed all membranes promoted cell adhesion, as shown by epifluorescence (Figs. 4 and 5). At day 1, cells grown on BC-Ap and BC-Ap OGP were adhered and showed predominantly roundish cell morphology, whereas cells cultured on BC-Ap OGP(10-14) or (BC-COL)-Ap with or without peptides exhibited a fusiform morphology (compare Figs. 4A–B to C and 5A–C). At day 3, cells grown on all membranes showed a well-spread morphology (Figs. 4D–F and 5D–F). Cell adhesion and spreading represents the first step of cell/material interactions and the features of this initial phase can influence the ability of cells to proliferate and to differentiate on the material surface [57]. Moreover, initial cell adhesion to the membrane may contribute to clot formation and wound stabilization, which is essential for GBR outcomes [58]. However, cells grown on BC-Ap, BC-Ap OGP and BC-Ap OGP(10-14) membranes showed a delay in cell adhesion and spreading in relation to the membranes of the Group II [(BC-COL)-Ap].

At day 7, BC-Ap and (BC-COL)-Ap showed a similar number of cells (compare Figs. 4G to 5G). In addition, the presence of OGP and OGP(10-14) peptides resulted in a large cell population, particularly on (BC-COL)-Ap, wherein cultured cells exhibited areas of cell multilayering (compare Figs. 4H–I to 5H–I). Overall, these results indicated that the collagen and apatite incorporation associated with OGP to the BC enhance cell growth at early time points, which is fundamental step for tissue regeneration [57].

Cell viability/proliferation were affected by composition of membranes at day 10 as follows: (BC-COL)-Ap = (BC-COL)-Ap OGP = BC-Ap > (BC-COL)-Ap OGP(10-14) > BC-Ap OGP (10-14) > BC-Ap OGP ($p < 0.001$). At day 14, great levels of cell viability/proliferation were observed for cultures grown on BC-Ap OGP, (BC-COL)-Ap, and (BC-COL)-Ap OGP(10-14) when compared with other membranes ($p < 0.001$; Fig. 6A).

At day 14, total protein content was higher for cells cultures on BC-Ap and (BC-COL)-Ap OGP than (BC-COL)-Ap and BC-Ap OGP(10-14) ($p < 0.001$). High values of total protein content were also noticed for cultures grown on BC-Ap OGP than BC-Ap OGP(10-14) ($p < 0.001$; Fig. 6B). No differences were observed for all membranes at day 17 ($p > 0.05$; Fig. 6B).

ALP activity was used as a marker for early osteoblastic cell differentiation, once its expression only takes place at the end of proliferative phase [59]. Moreover, ALP provides the inorganic phosphate (Pi) needed for matrix mineralization, and addition-

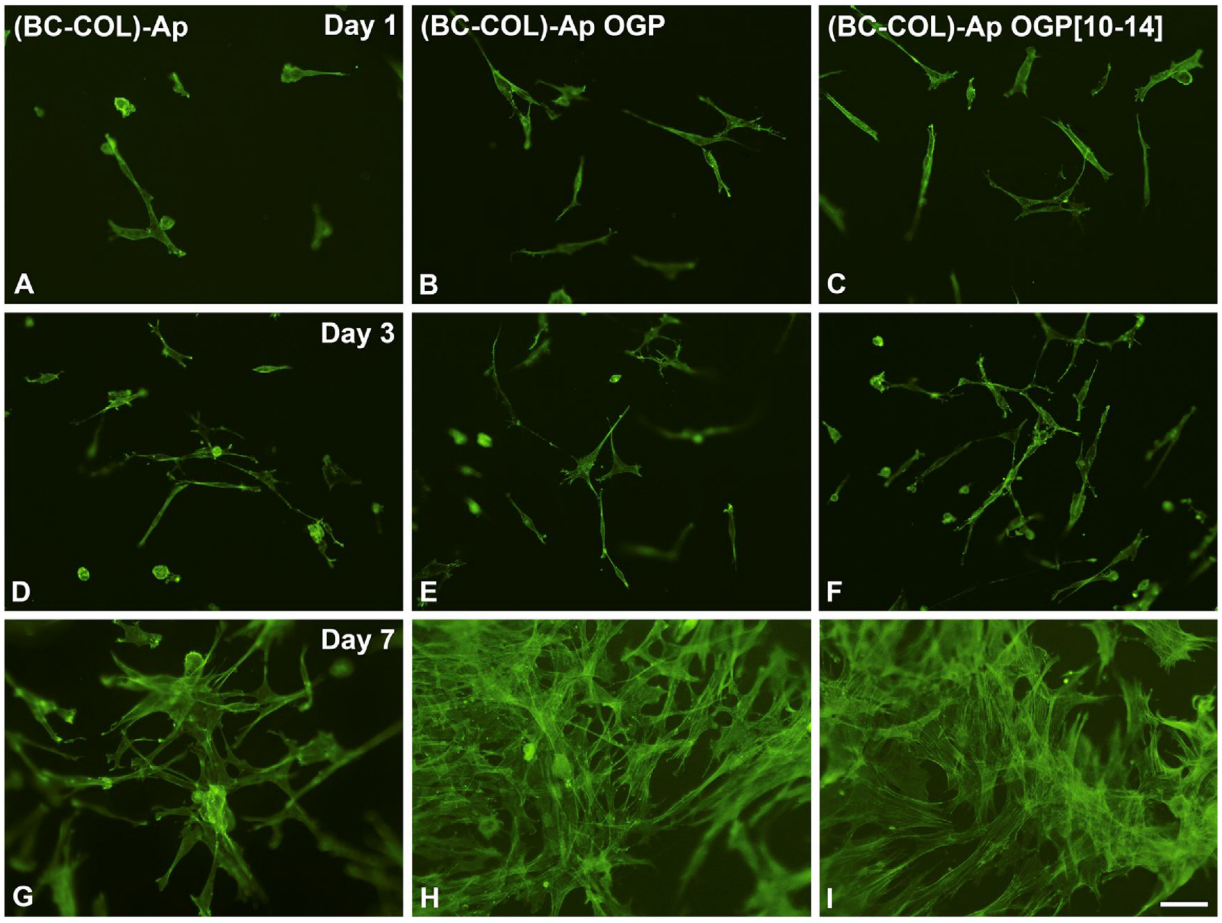

Fig. 5. Epifluorescence of osteoblastic cells cultured on (BC-COL)-Ap (A, D, G), (BC-COL)-Ap OGP (B, E, H), and (BC-COL)-Ap OGP(10-14) (C, F, I) at 1 (A-C), 3 (D-F) and 7 (G-I) days. Green fluorescence (Alexa Fluor 488-conjugated phalloidin) reveals actin cytoskeleton. At day 1, cells were adhered and exhibited fusiform shape on all membranes (A-C). At day 3, cell spreading was clearly noticed for all membranes (D–F). At day 7, a reduced number of cells was observed for cultures grown on (BC-COL)-Ap, while cells on other membranes showed areas of cell multilayering (compare G to H and I). Bar: A–F = 100 μm. (For interpretation of the references to colour in this figure legend, the reader is referred to the web version of this article.)

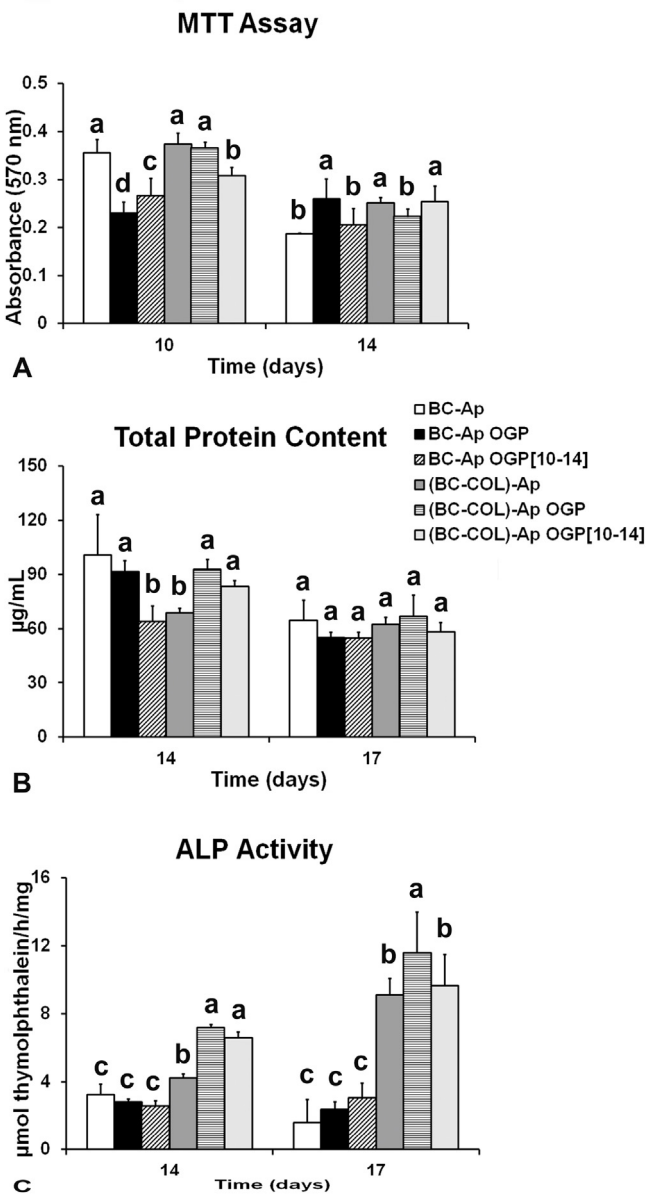

Fig. 6. Osteoblastic cells cultured on BC-Ap and (BC-COL)-Ap associated or not with osteogenic peptides. Cell viability/proliferation (A) was expressed as absorbance at days 10 and 14. Total protein content (B) was expressed as micrograms of protein per milliliter at days 14 and 17. ALP activity (C) was expressed as micromolar of thymolphthalein per hour per milligram of protein at days 14 and 17. Different letters indicate statistical significance for comparisons among the membranes in each experimental times ($p < 0.05$). Data are reported as mean ± SD.

ally acts as a signal for expression of important non-collagenous proteins, as osteopontin [60,61]. At day 14, ALP activity was higher for cells cultured on (BC-COL)-Ap OGP and (BC-COL)-Ap OGP(10-14) than BC-Ap associated or not with peptides ($p < 0.001$). At day 14, OGP and OGP(10-14) peptides incorporated into the (BC-COL)-Ap did not show statistical difference between them, although a tendency towards higher values of ALP activity was noticed for cultures grown on (BC-COL)-Ap OGP (Fig. 6C). At day 17, however, higher values of ALP activity were noticed for cultures grown on (BC-COL)-Ap OGP ($p < 0.001$; Fig. 6C).

Advances in material engineering have considered the synthesis of materials able to carry molecules controlling the cellular response and new-tissue development [62]. Several peptides and proteins implicated in cell signaling have a biological activity that makes them suitable for therapeutic purposes. These synthetic molecules include both growth factors and peptides which mimic whole proteins [63].

In this work, the incorporation of OGP and OGP(10-14) peptides to composites increase cell proliferation at initial time points, especially for cultures grown (BC-COL)-Ap associated with the OGP peptide, as revealed by epifluorescence. Moore et al. [64] also noticed an increase in cell proliferation of MC3T3-E1 cells exposed to the OGP compared with the OGP(10-14).

OGP and OGP(10-14) peptides when systemically administered by daily therapeutic doses display the property of accelerating the bone defects and fractures repair process. In addition, these peptides provide a faster transition from immature bone to lamellar with higher trabecular bone mass into repaired bone defects [29,33,34,65]. Nevertheless, few studies have been developed about drug delivery systems using OGP and OGP(10-14) peptides [18,21,36–38,66]. Shuqiang et al. [36] revealed that OGP-containing PLGA scaffolds were more effective than OGP-free scaffolds for bone repair even though the control group animals (OGP-free scaffolds) have daily received OGP by via systemic. These findings showed that local effect of the peptide was more effective than by systemic administration. Otherwise, OGP-containing different biomaterials such as, BC-HA membranes [21], poly(ester urea)-based scaffolds [37,66] and alginate hydrogel [38] have demonstrated effective results for applications in bone regeneration. The OGP-containing BC-HA membranes induced bone neoformation in critical-size calvarial defects mainly in early stages of bone regeneration in mice [21]. In subcutaneous rat model, the OGP-functionalized poly(ester urea) scaffolds exhibited a significant tissue-scaffold integration and enhanced proliferative activity, besides promoting both osteogenesis and angiogenesis effects [37,66]. Furthermore, injectable OGP–alginate hydrogels laden with human mesenchymal stem cells (hMSCs) induced an ectopic effect with cell proliferation and mineralization an endogenous extracellular matrix [38].

Additionally, OGP peptide associated with BC membranes showed a higher osteogenic cell proliferation in relation to OGP(10-14) on primary osteogenic cell cultures, wherein OGP peptide induced the mineralization process conferring an osteoinductive property to the BC membrane [18].

An increase in ALP activity has been reported in osteoblastic and marrow stromal cell cultures exposed to OGP and OGP(10-14) peptides [67,68]. Herein, cell viability/proliferation on cultures grown in the presence of both peptides were reduced in the Group II, and a higher protein deposition and ALP activity were noticed for same membranes groups compared with BC-Ap, at later times of culture. Indeed, the inverse relationship between cell proliferation and the process of cell differentiation is well known for osteoblastic lineage [59,67]. Despite of recognized effects of the OGP peptide on osteoblastic cells, a few works have been evaluated the *in vivo* effects of OGP incorporate to scaffolds/membranes [21,36–38,66].

In addition, the BC-Ap nanocomposites promoted a delay in the cell adhesion, spreading and proliferation. The results showed that the collagen improved biological properties of the composites promoting the osteoblastic differentiation, mainly in the presence of the peptides. Indeed, nanocomposites associated with OGP were able to induce the early development of osteoblastic phenotype. Additionally, the inorganic phase incorporated into (BC-COL)-Ap (carbonate apatite) induced a better response to osteoblastic differentiation, *i.e.*, a better response of ALP enzyme than BC-Ap nanocomposites. Thus, (BC-COL)-Ap nanocomposite might be a potential carrier for OGP peptide. Further, *in vivo* studies should be carried out to confirm whether the (BC-COL)-Ap OGP nanocomposite would be able to induce and improve the bone neoformation in GBR.

4. Conclusions

The composite based on BC, type I collagen and carbonate apatite demonstrated *in vitro* bioactivity and osteoinductive properties associated with OGP or its C-terminal pentapeptide OGP(10-14). The physicochemical characterizations revealed that *in situ* apatite synthesis at room temperature was an effective route for obtaining of these nanocomposites, suggesting the formation of bone-like apatite. In addition, composites exhibited a homogeneous nanostructure regarding the collagen and apatite incorporation. Moreover, gamma radiation was suitable method for sterilization of the materials, whereas this protocol maintained the thermal stability of the composites. These composites did not exhibit cytotoxicity, genotoxicity or mutagenicity effects. Furthermore, *in vitro* assays showed that the synergism between collagen and apatite associated with peptides (OGP or OGP(10-14)) induced cell growth at early time points regarding the BC-Ap nanocomposite. OGP peptide was capable to induce the early development of osteoblastic phenotype. These promising results suggest that the (BC-COL)-Ap associated with OGP peptides might be considered a potential candidate for bone tissue engineering applications.

Funding

This work was supported by the São Paulo Research Foundation – FAPESP, São Paulo, SP [Scholarship: 08/58776-6 and Grant number: 09/09960-1].

Acknowledgements

The authors wish to thank Prof. Dr. Luiz Geraldo Vaz of Department of Dental Materials and Prosthodontics, School of Dentistry at Araraquara – UNESP for support in the mechanical testing, and Mr Roger Rodrigues Fernandes of Cell Culture Laboratory, Faculty of Dentistry of Ribeirão Preto, University of São Paulo – USP for technical support.

Appendix A. Supplementary data

Supplementary data associated with this article can be found, in the online version, at http://dx.doi.org/10.1016/j.ijbiomac.2017.05.086.

References

[1] S. Saska, L.S. Mendes, A.M.M. Gaspar, T.S.d.O. Capote, Bone substitute materials in implant dentistry, in: I. Turkyilmaz (Ed.), Current Concepts in Dental Implantology, INTECH, Crotia, 2015, pp. 158–167.
[2] H.S. Barud, J. Gutierrez, W.R. Lustri, M.F.S. Peres, S.J.L. Ribeiro, S. Saska, A. Tercjak, Bacterial cellulose, in: N.M. Neves, R.L. Reis (Eds.), Biomaterials from Nature for Advanced Devices and Therapies, John Wiley & Sons, Inc, Hoboken, New Jersey, 2016, pp. 384–394.
[3] H. Ullah, F. Wahid, H.A. Santos, T. Khan, Advances in biomedical and pharmaceutical applications of functional bacterial cellulose-based nanocomposites, Carbohydr. Polym. 150 (2016) 330–352.
[4] W.K. Czaja, D.J. Young, M. Kawecki, R.M. Brown, The future prospects of microbial cellulose in biomedical applications, Biomacromolecules 8 (2007) 1–12.
[5] C. Zhijiang, Y. Guang, Bacterial cellulose/collagen composite: characterization and first evaluation of cytocompatibility, J. Appl. Polym. Sci. 120 (2011) 2938–2944.
[6] S.A. Hutchens, R.S. Benson, B.R. Evans, H.M. O'Neill, C.J. Rawn, Biomimetic synthesis of calcium-deficient hydroxyapatite in a natural hydrogel, Biomaterials 27 (2006) 4661–4670.
[7] B. Fang, Y.Z. Wan, T.T. Tang, C. Gao, K.R. Dai, Proliferation and osteoblastic differentiation of human bone marrow stromal cells on hydroxyapatite/bacterial cellulose nanocomposite scaffolds, Tissue Eng. Part A 15 (2009) 1091–1098.
[8] C.J. Grande, F.G. Torres, C.M. Gomez, M.C. Bano, Nanocomposites of bacterial cellulose/hydroxyapatite for biomedical applications, Acta Biomater. 5 (2009) 1605–1615.
[9] C. Gao, G.Y. Xiong, H.L. Luo, K.J. Ren, Y. Huang, Y.Z. Wan, Dynamic interaction between the growing Ca-P minerals and bacterial cellulose nanofibers during early biomineralization process, Cellulose 17 (2010) 365–373.
[10] S. Saska, H.S. Barud, A.M.M. Gaspar, R. Marchetto, S.J.L. Ribeiro, Y. Messaddeq, Bacterial cellulose-hydroxyapatite nanocomposites for bone regeneration, Int. J. Biomater. (2011) 8, http://dx.doi.org/10.1155/2011/175362, Article ID 175362.
[11] J. Wang, Y.Z. Wan, J. Han, X.W. Lei, T. Yan, C.A. Gao, Nanocomposite prepared by immobilising gelatin and hydroxyapatite on bacterial cellulose nanofibres, Micro Nano Lett. 6 (2011) 133–136.
[12] C. Wiegand, P. Elsner, U.C. Hipler, D. Klemm, Protease and ROS activities influenced by a composite of bacterial cellulose and collagen type I in vitro, Cellulose 13 (2006) 689–696.
[13] H.L. Luo, G.Y. Xiong, Y. Huang, F. He, W. Wang, Y.Z. Wan, Preparation and characterization of a novel COL/BC composite for potential tissue engineering scaffolds, Mater. Chem. Phys. 110 (2008) 193–196.
[14] S. Saska, L.N. Teixeira, P.T. de Oliveira, A.M.M. Gaspar, S.J.L. Ribeiro, Y. Messaddeq, R. Marchetto, Bacterial cellulose-collagen nanocomposite for bone tissue engineering, J. Mater. Chem. 22 (2012) 22102–22112.
[15] N. Nwe, T. Furuike, H. Tamura, Selection of a biopolymer based on attachment, morphology and proliferation of fibroblast NIH/3T3 cells for the development of a biodegradable tissue regeneration template: alginate, bacterial cellulose and gelatin, Process Biochem. 45 (2010) 457–466.
[16] H.G. Oliveira Barud, S. Barud Hda, M. Cavicchioli, T.S. do Amaral, O.B. de Oliveira, D.M. Santos, A.L. Petersen, F. Celes, V.M. Borges, C.I. de Oliveira Junior, P.F. de Oliveira, R.A. Furtado, D.C. Tavares, S.J. Ribeiro, Preparation and characterization of a bacterial cellulose/silk fibroin sponge scaffold for tissue regeneration, Carbohydr. Polym. 128 (2015) 41–51.
[17] H. Fink, L. Ahrenstedt, A. Bodin, H. Brumer, P. Gatenholm, A. Krettek, B. Risberg, Bacterial cellulose modified with xyloglucan bearing the adhesion peptide RGD promotes endothelial cell adhesion and metabolism-a promising modification for vascular grafts, J. Tissue Eng. Regen. Med. 5 (2011) 454–463.
[18] S. Saska, R.M. Scarel-Caminaga, L.N. Teixeira, L.P. Franchi, R.A. dos Santos, A.M. Minarelli Gaspar, P.T. de Oliveira, A.L. Rosa, C.S. Takahashi, Y. Messaddeq, S.J. Lima Ribeiro, R. Marchetto, Characterization and in vitro evaluation of bacterial cellulose membranes functionalized with osteogenic growth peptide for bone tissue engineering, J. Mater. Sci. Mater. Med. 23 (2012) 2253–2266.
[19] Q. Shi, Y. Li, J. Sun, H. Zhang, L. Chen, B. Chen, H. Yang, Z. Wang, The osteogenesis of bacterial cellulose scaffold loaded with bone morphogenetic protein-2, Biomaterials 33 (2012) 6644–6649.
[20] G.F. Picheth, M.R. Sierakowski, M.A. Woehl, L. Ono, A.R. Cofre, L.P. Vanin, R. Pontarolo, R.A. De Freitas, Lysozyme-triggered epidermal growth factor release from bacterial cellulose membranes controlled by smart nanostructured films, J. Pharm. Sci. 103 (2014) 3958–3965.
[21] S.C. Pigossi, G.J.P.L. De Oliveira, L.S. Finoti, R. Nepomuceno, L.C. Spolidorio, C. Rossa, S.J.L. Ribeiro, S. Saska, R.M. Scarel-Caminaga, Bacterial cellulose-hydroxyapatite composites with osteogenic growth peptide (OGP) or pentapeptide OGP on bone regeneration in critical-size calvarial defect model, J. Biomed. Mater. Res. A 103 (2015) 3397–3406.
[22] F. Goncalves, M.S. de Moraes, L.B. Ferreira, A.C. Carreira, P.M. Kossugue, L.C. Boaro, R. Bentini, C.R. Garcia, M.C. Sogayar, V.E. Arana-Chavez, L.H. Catalani, Combination of bioactive polymeric membranes and stem cells for periodontal regeneration: in vitro and in vivo analyses, PLoS One 11 (2016) e0152412.
[23] M.M. Villa, L. Wang, J. Huang, D.W. Rowe, M. Wei, Improving the permeability of lyophilized collagen-hydroxyapatite scaffolds for cell-based bone regeneration with a gelatin porogen, J. Biomed. Mater. Res. B Appl. Biomater. 104 (2016) 1580–1590.
[24] J.H. Song, H.E. Kim, H.W. Kim, Collagen-apatite nanocomposite membranes for guided bone regeneration, J. Biomed. Mater. Res. B Appl. Biomater. 83 (2007) 248–257.
[25] S. Yunoki, E. Marukawa, T. Ikoma, S. Sotome, H. Fan, X. Zhang, K. Shinomiya, J. Tanaka, Effect of collagen fibril formation on bioresorbability of hydroxyapatite/collagen composites, J. Mater. Sci. Mater. Med. 18 (2007) 2179–2183.
[26] S. Liao, W. Wang, M. Uo, S. Ohkawa, T. Akasaka, K. Tamura, F. Cui, F. Watari, A three-layered nano-carbonated hydroxyapatite/collagen/PLGA composite membrane for guided tissue regeneration, Biomaterials 26 (2005) 7564–7571.
[27] S.H. Teng, E.J. Lee, P. Wang, D.S. Shin, H.E. Kim, Three-layered membranes of collagen/hydroxyapatite and chitosan for guided bone regeneration, J. Biomed. Mater. Res. B Appl. Biomater. 87 (2008) 132–138.
[28] J.B. Matson, R.H. Zha, S.I. Stupp, Peptide self-assembly for crafting functional biological materials, Curr. Opin. Solid State Mater. Sci. 15 (2011) 225–235.
[29] I. Bab, D. Gazit, M. Chorev, A. Muhlrad, A. Shteyer, Z. Greenberg, M. Namdar, A. Kahn, Histone H4-related osteogenic growth peptide (OGP)—a novel circulating stimulator of osteoblastic activity, EMBO J. 11 (1992) 1867–1873.
[30] I. Bab, M. Chorev, Osteogenic growth peptide: from concept to drug design, Biopolymers 66 (2002) 33–48.
[31] O. Gurevitch, S. Slavin, A. Muhlrad, A. Shteyer, D. Gazit, M. Chorev, M. Vidson, M. NamdarAttar, E. Berger, I. Bleiberg, I. Bab, Osteogenic growth peptide increases blood and bone marrow cellularity and enhances engraftment of bone marrow transplants in mice, Blood 88 (1996) 4719–4724.
[32] Z. Greenberg, H. Gavish, A. Muhlrad, M. Chorev, A. Shteyer, M. AttarNamdar, A. Tartakovsky, I. Bab, Isolation of osteogenic growth peptide from osteoblastic MC3T3-E1 cell cultures and demonstration of osteogenic growth peptide binding proteins, J. Cell. Biochem. 65 (1997) 359–367.

[33] Y.Q. Sun, D.E. Ashhurst, Osteogenic growth peptide enhances the rate of fracture healing in rabbits, Cell Biol. Int. 22 (1998) 313–319.
[34] Y. Gabet, R. Muller, E. Regev, J. Sela, A. Shteyer, K. Salisbury, M. Chorev, I. Bab, Osteogenic growth peptide modulates fracture callus structural and mechanical properties, Bone 35 (2004) 65–73.
[35] Z.Y. Zhao, L. Shao, H.M. Zhao, Z.H. Zhong, J.Y. Liu, C.G. Hao, Osteogenic growth peptide accelerates bone healing during distraction osteogenesis in rabbit tibia, J. Int. Med. Res. 39 (2011) 456–463.
[36] M. Shuqiang, W. Kunzheng, D. Xiaoqiang, W. Wei, Z. Mingyu, W. Daocheng, Osteogenic growth peptide incorporated into PLGA scaffolds accelerates healing of segmental long bone defects in rabbits, J. Plast Reconstr. Aesthet. Surg. 61 (2008) 1558–1560.
[37] K.S. Stakleff, F. Lin, L.A. Smith Callahan, M.B. Wade, A. Esterle, J. Miller, M. Graham, M.L. Becker, Resorbable, amino acid-based poly(ester urea)s crosslinked with osteogenic growth peptide with enhanced mechanical properties and bioactivity, Acta Biomater. 9 (2013) 5132–5142.
[38] F.R. Maia, M. Barbosa, D.B. Gomes, N. Vale, P. Gomes, P.L. Granja, C.C. Barrias, Hydrogel depots for local co-delivery of osteoinductive peptides and mesenchymal stem cells, J. Controlled Release 189 (2014) 158–168.
[39] D. Massiot, F. Fayon, M. Capron, I. King, S. Le Calve, B. Alonso, J.O. Durand, B. Bujoli, Z. Gan, G. Hoatson, Modelling one- and two-dimensional soli-state NMR spectra, Magn. Reson. Chem. 40 (2002) 70–76.
[40] T.T. Nge, J. Sugiyama, Surface functional group dependent apatite formation on bacterial cellulose microfibrils network in a simulated body fluid, J. Biomed. Mater. Res. A 81 (2007) 124–134.
[41] A. Kaflak, W. Kolodziejski, Kinetics $^{1}H \rightarrow ^{31}P$ NMR cross-polarization in bone apatite and its mineral standards, Magn. Reson. Chem. 46 (2008) 335–341.
[42] Y.Y. Hu, Y. Yusufoglu, M. Kanapathipillai, C.Y. Yang, Y.Q. Wu, P. Thiyagarajan, T. Deming, M. Akinc, K. Schmidt-Rohr, S. Mallapragada, Self-assembled calcium phosphate nanocomposites using block copolypeptide templates, Soft Matter 5 (2009) 4311–4320.
[43] X. Su, K. Sun, F.Z. Cui, W.J. Landis, Organization of apatite crystals in human woven bone, Bone 32 (2003) 150–162.
[44] Y.Z. Wan, Y. Huang, C.D. Yuan, S. Raman, Y. Zhu, H.J. Jiang, F. He, C. Gao, Biomimetic synthesis of hydroxyapatite/bacterial cellulose nanocomposites for biomedical applications, Mater. Sci. Eng. C 27 (2007) 855–864.
[45] G.R. Sauer, R.E. Wuthier, Fourier transform infrared characterization of mineral phases formed during induction of mineralization by collagenase-released matrix vesicles in vitro, J. Biol. Chem. 263 (1988) 13718–13724.
[46] Y.H. Tseng, C.Y. Mou, J.C.C. Chan, Solid-state NMR study of the transformation of octacalcium phosphate to hydroxyapatite: a mechanistic model for central dark line formation, J. Am. Chem. Soc. 128 (2006) 6909–6918.
[47] Y.H. Tseng, Y.L. Tsai, T.W.T. Tsai, J.C.H. Chao, C.P. Lin, S.H. Huang, C.Y. Mou, J.C.C. Chan, Characterization of the phosphate units in rat dentin by solid-state NMR spectroscopy, Chem. Mater. 19 (2007) 6088–6094.
[48] W.E. Brown, Crystal growth of bone mineral, Clin. Orthop. Relat. Res. 44 (1966) 205–220.
[49] P. Bodier-Houlle, P. Steuer, J.C. Voegel, F.J. Cuisinier, First experimental evidence for human dentine crystal formation involving conversion of octacalcium phosphate to hydroxyapatite, Acta Crystallogr. D Biol. Crystallogr. 54 (1998) 1377–1381.
[50] R.Z. Legeros, Calcuim Phophastes in Oral Biology and Medicine, Karger, Basel, 1991.
[51] R.N. Panda, M.F. Hsieh, R.J. Chung, T.S. Chin, X.R.D. FTIR, SEM and solid state NMR investigations of carbonate-containing hydroxyapatite nano-particles synthesized by hydroxide-gel technique, J. Phys. Chem. Solids 64 (2003) 193–199.
[52] Y.H. Tseng, Y. Mou, P.H. Chen, T.W.T. Tsai, C.I. Hsieh, C.Y. Mou, J.C.C. Chan, Solid-state ^{31}P NMR study of the formation of hydroxyapatite in the presence of glutaric acid, Magn. Reson. Chem. 46 (4) (2008) 330–334.
[53] M.J. Duer, The molecular glue binding organic matrix and mineral crystals in biominerals: bask amino acids may be as important as acidic ones A perspective on the role of basic amino acids in the molecular recognition of hydroxyapatite by statherin using solid state NMR by M. Ndao, J.T. Ash, P. Stayton, G. Drobny, Surf. Sci. 604 (2010) 1237–1238.
[54] L. Szcześniak, A. Rachocki, J. Tritt-Goc, Glass transition temperature and thermal decomposition of cellulose powder, Cellulose 15 (3) (2008) 445–451.
[55] M. Coïc, V. Placet, E. Jacquet, C. Meyer, Mechanical properties of collagen membranes used in guided bone regeneration: a comparative study of three models, Rev. Stomatol. Chir. Maxillofac. 111 (2010) 286–290.
[56] A. Spreafico, B. Frediani, C. Capperucci, A. Leonini, D. Gambera, P. Ferrata, S. Rosini, A. Di Stefano, M. Galeazzi, R. Marcolongo, Osteogenic growth peptide effects on primary human osteoblast cultures: potential relevance for the treatment of glucocorticoid-induced osteoporosis, J. Cell. Biochem. 98 (2006) 1007–1020.
[57] K. Anselme, Osteoblast adhesion on biomaterials, Biomaterials 21 (2000) 667–681.
[58] A. Kasaj, C. Reichert, H. Gotz, B. Rohrig, R. Smeets, B. Willershausen, In vitro evaluation of various bioabsorbable and nonresorbable barrier membranes for guided tissue regeneration, Head Face Med. 4 (2008) 22.
[59] T.A. Owen, M. Aronow, V. Shalhoub, L.M. Barone, L. Wilming, M.S. Tassinari, M.B. Kennedy, S. Pockwinse, J.B. Lian, G.S. Stein, Progressive development of the rat osteoblast phenotype in vitro: reciprocal relationships in expression of genes associated with osteoblast proliferation and differentiation during formation of the bone extracellular matrix, J. Cell. Physiol. 143 (1990) 420–430.
[60] G.R. Beck Jr., B. Zerler, E. Moran, Phosphate is a specific signal for induction of osteopontin gene expression, Proc. Natl. Acad. Sci. U. S. A. 97 (2000) 8352–8357.
[61] Y. Sugawara, K. Suzuki, M. Koshikawa, M. Ando, J. Iida, Necessity of enzymatic activity of alkaline phosphatase for mineralization of osteoblastic cells, Jpn. J. Pharmacol. 88 (2002) 262–269.
[62] J.K. Tessmar, A.M. Gopferich, Matrices and scaffolds for protein delivery in tissue engineering, Adv. Drug Deliv. Rev. 59 (2007) 274–291.
[63] W. Mark Saltzman, S.P. Baldwin, Materials for protein delivery in tissue engineering, Adv. Drug Deliv. Rev. 33 (1998) 71–86.
[64] N.M. Moore, N.J. Lin, N.D. Gallant, M.L. Becker, The use of immobilized osteogenic growth peptide on gradient substrates synthesized via click chemistry to enhance MC3T3-E1 osteoblast proliferation, Biomaterials 31 (2010) 1604–1611.
[65] Y.C. Chen, I. Bab, N. Mansur, A. Muhlrad, A. Shteyer, M. Namdar-Attar, H. Gavish, M. Vidson, M. Chorev, Structure-bioactivity of C-terminal pentapeptide of osteogenic growth peptide [OGP(10-14)], J. Pept. Res. 56 (2000) 147–156.
[66] G.M. Policastro, F. Lin, L.A. Smith Callahan, A. Esterle, M. Graham, K. Sloan Stakleff, M.L. Becker, OGP functionalized phenylalanine-based poly(ester urea) for enhancing osteoinductive potential of human mesenchymal stem cells, Biomacromolecules 16 (2015) 1358–13571.
[67] D. Robinson, I. Bab, Z. Nevo, Osteogenic growth peptide regulates proliferation and osteogenic maturation of human and rabbit bone marrow stromal cells, J. Bone Miner. Res. 10 (1995) 690–696.
[68] Z. Chen, X. Wang, Y. Shao, D. Shi, T. Chen, D. Cui, X. Jiang, Synthetic osteogenic growth peptide promotes differentiation of human bone marrow mesenchymal stem cells to osteoblasts via RhoA/ROCK pathway, Mol. Cell. Biochem. 358 (2011) 221–227.